

# Fabrication and characterization of nanostructural WS<sub>2</sub>/WO<sub>3</sub> binary compound semiconductors prepared by the sulfurization of sprayed thin films

M. Adelifard<sup>1</sup> · R. Salamatizadeh<sup>1</sup> · S. A. Ketabi<sup>1</sup>

Received: 29 December 2015 / Accepted: 25 January 2016 / Published online: 1 February 2016  
© Springer Science+Business Media New York 2016

**Abstract** We have investigated the impact of sulfurization and changing the metal salt ratio ( $[s]/[w] = 6\text{--}24$  at.%) in the precursor solution on the structural, morphological, optical, electrical and photoconductivity properties of WS<sub>2</sub>/WO<sub>3</sub> binary thin films grown on glass substrate by the spray pyrolysis technique. X-ray diffraction analysis showed that while the as-deposited samples present an amorphous nature, annealing these films in sulfur atmosphere generate a mix phase of WS<sub>2</sub>/WO<sub>3</sub>. FESEM study revealed the changes in surface morphology with increase in sulfur concentration in the spray solution. UV–Vis optical measurements analysis showed that these binary films have a relatively high absorption coefficient  $\sim 2 \times 10^4\text{--}8 \times 10^4$  cm<sup>-1</sup> in the visible spectrum with two distinct inflexions indicative of two transitions correspond to WS<sub>2</sub>/WO<sub>3</sub> phases in agreement with the XRD analysis. The electrical studies showed that all these samples have a p-type conductivity; and the resistivity and photoconductivity decreases with increasing the sulfur to tungsten molar ratio.

## 1 Introduction

Tungsten trioxide (WO<sub>3</sub>) belongs to a class of transition metal oxides, has been the most extensively studied material due to its electrochromic properties in the visible and infrared region, high coloration efficiency and relatively low price [1]. It is used for the construction of smart windows [2], mirrors, optical shutters and display devices [3], etc. Up to now, several techniques for the growth of

WO<sub>3</sub> thin films have been reported: thermal evaporation [4], flash evaporation [5], electron beam [6], spray pyrolysis [7], sputtering [8], and sol–gel coating [9].

On the other hand, studies of transition metal disulfides MS<sub>2</sub> (M = Ti, Zr, Hf, V, Nb, Ta, Mo, and W) have received an ever increasing attention. Among them, tungsten disulfide (WS<sub>2</sub>) with unique properties is a promising material for number of applications such as solid lubricant, catalyst, photo sensitive films [10], electronic devices [11], super shock absorbers [12], etc. WS<sub>2</sub> crystallize into a layered structure, in which atoms forming each layer are covalently bonded while adjacent layers are held weakly by van der Waals (VDW) forces. Different methods have been used to prepare WS<sub>2</sub> thin films, e.g. chemical vapor deposition (CVD) [13, 14], radiofrequency sputtering [15], activated reactive evaporation [16], electrodeposition [17], sulfurization of WO<sub>3</sub> thin films [18], etc.

An important task of modern material science is the creation of new multicomponent semiconductor materials as the physical properties of which can be controlled by varying their composition. The synthesis of binary and ternary technological semiconductors can be opens up significant opportunities in nanoscale science and technology. However, few attempts have been made to prepare binary system of transition metal sulfides/transition metal oxides. The basis of our knowledge only one report on the preparation of WS<sub>2</sub>/WO<sub>3</sub> thin films was available. Jana et al. [19] have used electrodeposition technique to synthesize WS<sub>2</sub> thin films on ITO (indium tin oxide) glass substrate. Air annealing the WS<sub>2</sub> thin films at 450 °C resulted a mix phase of WS<sub>2</sub>/WO<sub>3</sub> with better catalytic activity than other single phase thin films.

The present work reports the details of fabrication and characterization of WS<sub>2</sub>/WO<sub>3</sub> thin films prepared by sulfurization of sprayed thin films. We have investigated the

✉ M. Adelifard  
adelifard@du.ac.ir

<sup>1</sup> School of Physics, Damghan University, Damghan, Iran

corresponding samples from various viewpoints, including structural- (crystallinity and surface morphology), optical (UV–Vis–Near IR transmittance spectra/band gap estimation), electrical (carrier density, resistivity and mobility) and photoconductivity properties.

## 2 Experimental details

### 2.1 Sample preparation

In this research thin films were deposited on glass substrate by spray pyrolysis technique. The basis spray solution for any samples was prepared by solving 0.04 M (1.5864 g) of tungsten chloride ( $\text{WCl}_6$ ) in mixture of hydrazine hydrate ( $\text{N}_2\text{H}_4 \cdot \text{H}_2\text{O}$ ) and double distilled water in ratio of 1:10 (w/w). To enhance the solubility of tungsten chloride, a few drops of acetic acid was also added to the solution. Then thiourea [ $\text{SC}(\text{NH}_2)_2$ ] as the sulfur source (with various [S]/[W] molar ratio equal to 6.0–12, 18 and 24 at.%) in order to study on effect of sulfur concentration on physical properties of the studied samples was added to the basis solution. The final solution was stirred for 30 min to obtain a clear yellow solution. Before spraying the solution, the substrate temperature was set at 400 °C with an accuracy of  $\pm 5$  °C using a digital temperature controller for all samples. Other deposition parameters such as spray solution volume, spray deposition rate, the distance between nozzle and substrate and hot plate rotation speed were set at: 100 ml, 12 ml/min, 30 cm and 50 rpm, respectively.

#### 2.1.1 Annealing process of the sprayed thin films

Annealing of thin films produced by the spray technique in sulfur atmosphere then occurred in a three-heating-zone quartz-tube furnace using Argon and  $\text{H}_2$  as the carrying gases, as described in the following. In the inlet area of the furnace, sulfur powder was put for sulfurization of the films (placed in the middle area of furnace) and then the furnace was sealed. The temperature of initial, middle and output area of furnace was set on 150, 400 and 400 °C, respectively. Before the furnace was turned on, Argon gas was used to purge the quartz tube at 30 ml/min for 10 min. When the furnace was turned on,  $\text{H}_2$  gas flow to the quartz tube with rate of 25 ml/min while Argon gas (30 ml/min) was also introduced. The furnace reached to desired temperatures with a constant rate of 20 °C/min. These conditions were established for 60 min, and after that the furnace was turned off and  $\text{H}_2$  gas was interrupted, but Argon gas was flowed about 30 min to prevent oxidation. The final prepared thin films were denoted as ‘WS6’, ‘WS12’, ‘WS18’ and ‘WS24’ corresponding to sulfur to tungsten molar ratio of 6, 12, 18 and 24 at.%, respectively.

### 2.2 Characterization of thin films

An X-ray diffractometer (D8 Advance Bruker) was used to record X-ray diffraction (XRD) patterns using  $\text{Cu-K}_\alpha$  radiation ( $\lambda = 0.15406$  nm) spectra in the  $2\theta$  range 10–70°. Transmittance Spectra were recorded in the wavelength range 300–1100 nm by a Shimadzu UV1800 spectrophotometer.

The surface morphology was observed using a HITACHI S-4160 Field Emission Scanning Electron Microscope (FESEM).

The film thickness of studied samples were determined by gravimetric weight difference method. For this, a sensitive microbalance was used and film density was assumed as the bulk density of  $\text{WS}_2$  ( $7.5 \text{ g/cm}^3$ ).

To study the photoconductive properties of prepared films, samples were exposed to light radiation with fixed intensity (3500 lx) at a fixed distance (20 cm). Then, the resistance of films were recorded under lighting at specified time intervals at room temperature.

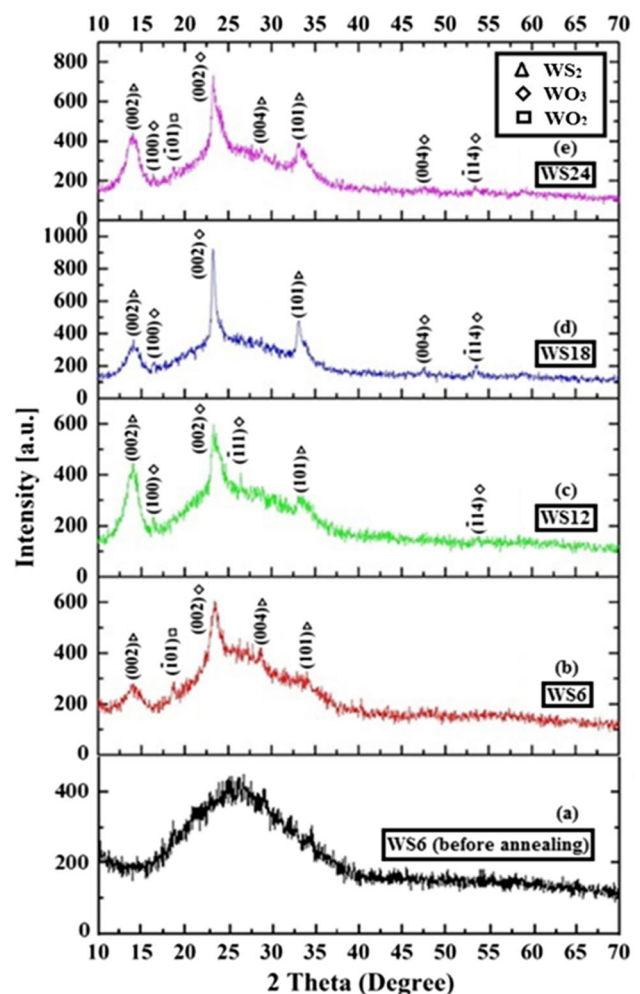


**Fig. 1** XRD pattern of *a* as-deposited thin film with [S]/[W] ratio of 6 and annealed thin films in sulfur atmosphere

Finally the electrical resistivity and Hall effect data (magnetic field strength = 200 mT) of the samples were measured in the Van der Pauw configuration [20].

### 3 Results and discussion

#### 3.1 Structural analysis

The structural analysis of the studied samples was carried out by using X-ray diffractometer with diffraction angle  $2\theta$  varied from  $10^\circ$  to  $70^\circ$ . The data analysis shows an amorphous nature for the sprayed film with ratio of  $S/W = 6$  at. % before annealing in sulfur atmosphere (Fig. 1a). Another sprayed thin films with different molar ratio of  $S/W$ ,

also yield the same result before annealing. With annealing of thin films produced by the spray technique in sulfur atmosphere (described in Sect. 2.1.1), as seen in (Fig. 1b, c, d, e) and Table 1, these layers show not only the  $WS_2$  structure in (002)–the preferred orientation, (004) and (101) directions whose  $2\theta$  values matches well with the standard JCPDS for the hexagonal structure (JCPDS Card No. 08-0237) of  $WS_2$ , but also the  $WO_3$  monoclinic structure characteristic peaks of (002)– the preferred orientation, (004) and  $(\bar{1}14)$  planes match well with standard JCPDS (JCPDS Card No. 87-2375). So annealing results are mix phases of  $WS_2/WO_3$  in all samples. The presence of another orientation along  $(\bar{1}01)$  which belong to  $WO_2$  monoclinic phase (JCPDS Card No. 32-1393) was also detected, but with substantially lower intensity.

**Table 1** Summary of the XRD parameters and mean crystallite size for different crystallographic orientations and various sulfur to tungsten molar ratios

hkl	$2\theta$ ( $^\circ$ )	Lattice distance (d) ( $\text{Å}$ )	Intensity (cp)	FWHM ( $^\circ$ )	Crystallite size (nm)	Identification with (hkl) valu
(a) WS6						
002	14.11	6.28	49	1.57	5.10	Hexagonal- $WS_2$
004	28.74	3.10	45	0.47	17.44	Hexagonal- $WS_2$
101	34.13	2.63	32	0.24	34.61	Hexagonal- $WS_2$
002*	23.48	3.79	214	0.82	9.90	Monoclinic- $WO_3$
$\bar{1}01$	18.70	4.74	54	0.31	25.96	Monoclinic- $WO_2$
(b) WS12						
002*	13.95	6.34	234	1.26	6.35	Hexagonal- $WS_2$
101	33.33	2.69	49	0.94	8.82	Hexagonal- $WS_2$
100	16.39	5.41	19	0.16	50.14	Monoclinic- $WO_3$
002	23.43	3.79	197	0.77	10.53	Monoclinic- $WO_3$
$\bar{1}11$	26.48	3.37	65	0.12	67.98	Monoclinic- $WO_3$
$\bar{1}14$	53.69	1.71	17	0.39	22.82	Monoclinic- $WO_3$
(c) WS18						
002	14.08	6.29	131	1.41	5.67	Hexagonal- $WS_2$
101	33.13	2.70	211	0.40	20.71	Hexagonal- $WS_2$
100	16.40	5.40	22	0.31	25.88	Monoclinic- $WO_3$
002*	23.26	3.82	547	0.31	26.15	Monoclinic- $WO_3$
004	47.47	1.91	25	0.47	18.46	Monoclinic- $WO_3$
$\bar{1}14$	53.55	1.71	48	0.31	28.69	Monoclinic- $WO_3$
(d) WS24						
002	13.97	6.48	202	1.26	6.35	Hexagonal- $WS_2$
004	28.88	3.09	25	0.47	17.45	Hexagonal- $WS_2$
101	33.13	2.70	105	0.68	12.18	Hexagonal- $WS_2$
100	16.38	5.41	27	0.31	25.88	Monoclinic- $WO_3$
002*	23.26	3.82	342	0.70	11.58	Monoclinic- $WO_3$
004	47.52	1.91	18	0.64	13.56	Monoclinic- $WO_3$
$\bar{1}14$	53.52	1.71	26	0.37	24.04	Monoclinic- $WO_3$
$\bar{1}01$	18.72	4.74	41	0.31	25.96	Monoclinic- $WO_2$

\* Characteristic peak of (002) is the preferred orientation in any sample

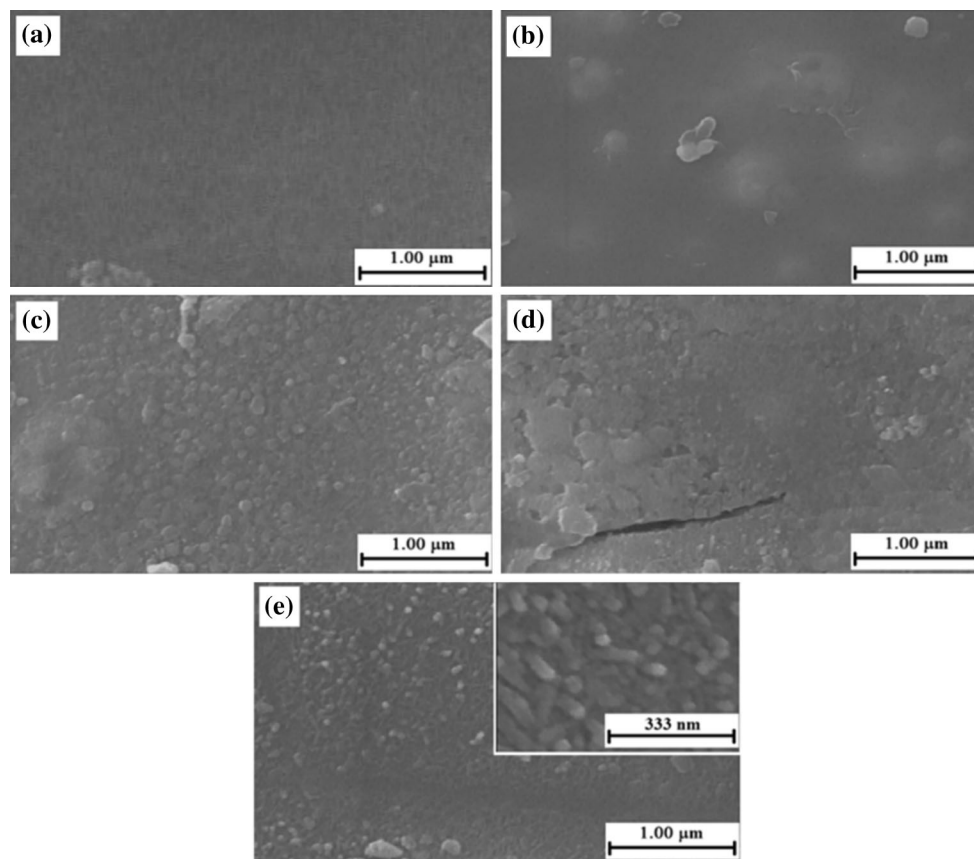


**Fig. 2** FESEM images of **a** as-deposited thin film with [S]/[W] ratio of 6, **b** WS6, **c** WS12, **d** WS18 and **e** WS24 thin films

Using Scherer's formula:

$$D = \frac{k\lambda}{\delta w \cos \theta} \quad (1)$$

where  $\lambda$  is the X-ray wavelength,  $\delta w$  is the full-width at half-maximum of the peak (FWHM),  $k$  is a constant (close to unity) and  $\theta$  is the Bragg angle; we found an estimation of the average crystallite size ( $D$ ) in the studied samples, see Table 1. Increasing [S]/[W] molar ratios, reduces the amorphous background, increases the preferred peak intensities and reduces their width, which results in crystallite size increase.

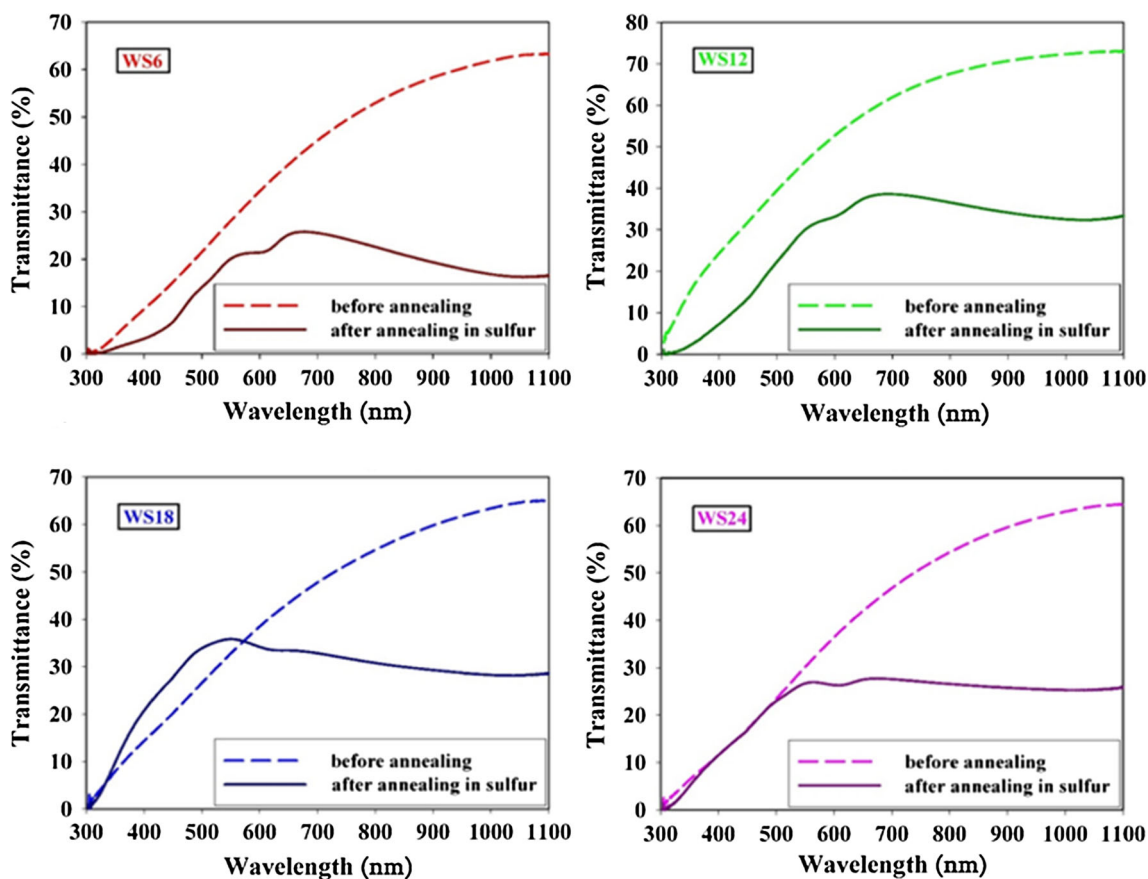
### 3.2 Morphological analyses by FESEM

Figure 2 depicts the FESEM images of the as-deposited and the annealed  $\text{WS}_2/\text{WO}_3$  samples. Whilst the spray deposited sample and its annealed (WS6 sample) showed relatively uniform, homogenous and amorphous compact structure (see Fig. 2a, b), a densely-packed structure with small grains was observed in the annealed samples with higher sulfur concentrations. This indicates a progressive improvement of the crystallinity after post annealing treatment in a sulfur atmosphere. Here, the WS12 sample,

Fig. 2c, showed a uniform distribution of nano-cubic like grain structure with the grain size of  $\sim 50$  nm. Beyond this S/W molar ratio, at  $S/W = 18$  at. %, overgrown impurities were observed. It is observed that surface morphological of WS24 thin film was much different from other samples. The low magnification image (Fig. 2e inset) shows that the product mainly consists of highly compact nano-rod structures. The average length of a nano-rod is  $<150$  nm with the diameter in a range 30–50 nm. The change in surface morphology at higher sulfur concentrations was due to the modification of grain growth into nanocrystalline with enhancement in the crystallinity. The variations in the surface morphology in these samples affected their optical and electrical properties, as described in the following.

### 3.3 Optical analysis

The optical transmittance of the as-deposited and the annealed samples were recorded in the wavelength range from 300 to 1100 nm, see Fig. 3. As it is evident while all as-deposited samples with various S/W molar ratios have a relatively high transmittances of  $\sim 70$  % around 1100 nm, transmission of the layers in general were found to decrease after annealing. It can be also noticed that the transmission



**Fig. 3** Optical transmittance spectra of the sprayed thin films with various sulfur to tungsten molar ratios before and after annealing in sulfur atmosphere

of the annealed layers (WS6–WS24 samples) were more remarkable around 560–670 nm in the visible region, while at the same time, a substantial decrease of transmission was found throughout the near infrared (NIR) region. The existence of shoulders near the fundamental absorption indicated the presence of different phases in the layers well matched with XRD analysis, see Fig. 1 and Table 1.

Figure 4 shows the optical absorption coefficient,  $\alpha(\lambda)$ , which was estimated using the data presented in Fig. 3, i.e. the transmittance measurements:

$$\alpha = \frac{1}{d} \ln\left(\frac{1}{T}\right) \tag{2}$$

where  $d$  is the thickness of the layers and are listed in Table 2. It was found that the studied samples presented high absorption coefficient values of about  $10^4 \text{ cm}^{-1}$ , see Fig. 4. The variation of absorption coefficient versus wavelength,  $\alpha(\lambda)$ , is linear indicating that the absorption near fundamental band edge is direct and allowed. The energy band gap of the films was evaluated using the relation [21]:

$$(\alpha h\nu)^{1/n} = A(h\nu - E_g) \tag{3}$$

where  $E_g$  is the energy band gap and  $n = 1/2$  for direct allowed transition. The plot of  $(\alpha h\nu)^2$  versus  $h\nu$  is a straight line and its x-intercept at  $(\alpha h\nu)^2 = 0$  gives the energy band gap of the material. The details of analysis of the direct band gaps can be found in the inset of the related graphs in Fig. 4. The as-deposited film formed at S/W ratio of 6 without annealing showed an optical band gap close to 2.46 eV whereas for those annealed layers in sulfur atmosphere (WS6–WS24 samples) observed that the plots are parabolic in nature, having two distinct inflexions which indicates two transitions occurring in thin films. The presence of two phases in the annealed films grown with various S/W molar ratios were identified using X-ray diffraction studies, see Fig. 1 and Table 1, and it supports the observed two transitions occurring in thin films. The higher energy bandgap values of the layers, i.e. 2.18–2.40 eV is due to the presence of  $\text{WO}_3$  phase, comparable with the values reported elsewhere, whilst the values of energy band gap in the range of 1.17–1.71 eV are belong to  $\text{WS}_2$  phase [19]. Shape, size, size distribution, phase, crystalline degree, and defects can play a role in the energy gaps of materials. Generally,  $E_g$  becomes wider by using smaller particles but narrower by the presence of defects.



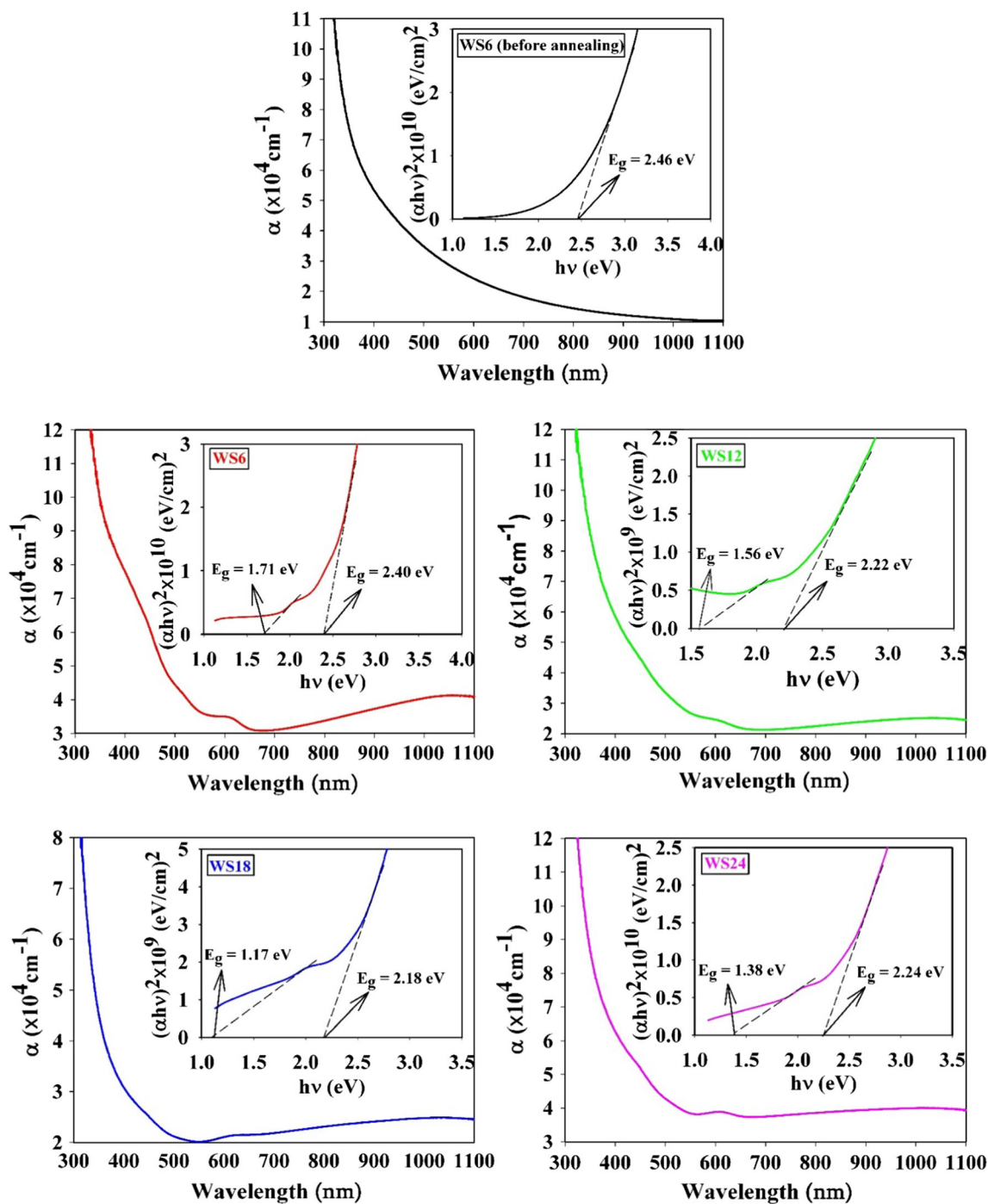


**Fig. 4** The optical absorption coefficient,  $\alpha(\lambda)$ , for as-deposited thin film and WS<sub>2</sub>/WO<sub>3</sub> thin films. (inset band gap photon energy,  $E_g$ )

**Table 2** Thickness and electrical measurement results of the WS<sub>2</sub>/WO<sub>3</sub> films for various sulfur concentrations

Sample	Thickness (nm)	Resistivity ( $\Omega \text{ cm}$ )	Carrier density ( $\text{cm}^{-3}$ )	Mobility ( $\text{cm}^2/\text{V s}$ )
WS6	441	512.5	$7.6 \times 10^{13}$	160.5
WS12	448	132.3	$0.7 \times 10^{15}$	66.5
WS18	510	142.4	$1.1 \times 10^{15}$	38.7
WS24	344	26.7	$6.0 \times 10^{15}$	38.8

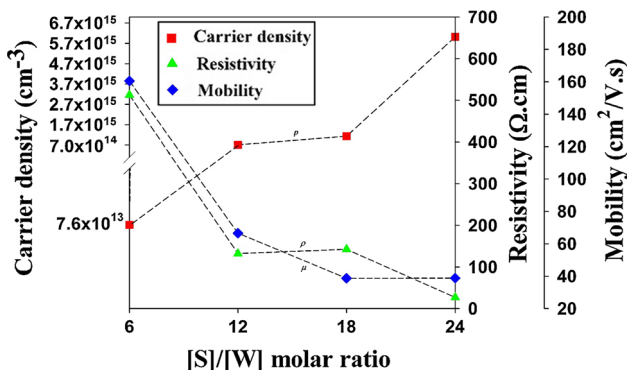


**Fig. 5** The variations of resistivity  $\rho$ , Hall mobility  $\mu$ , and carrier density  $p$  as a function of  $[S]/[W]$  ratio in  $WS_2/WO_3$  thin films

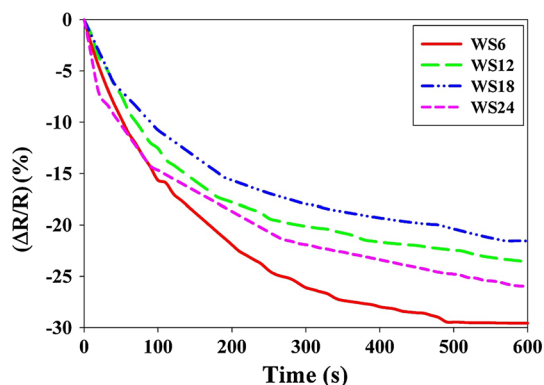


**Fig. 6** The relative reduction of resistance versus exposure time for  $WS_2/WO_3$  thin films

### 3.4 Electrical and photoconductivity properties

Figure 5 show the variations of Hall mobility ( $\mu$ ), carrier density ( $p$ ) and resistivity ( $\rho$ ) of the  $WS_2/WO_3$  thin films, and the results are given in Table 2. Through the Hall data acquisitions we found out that all the studied samples exhibited  $p$ -type conductivity. It is apparent from Fig. 5 that Hall mobility is decreasing with the increasing ratio of S/W till the ratio of 18 and then saturates for the higher molar ratio. This reduction in mobility values are attributed to grain boundary scattering and ionized impurity scattering, compatible with the shifts in the transmittance spectra shown in Fig. 3 in relation with their poor/rich metallic-like behavior. The resistivity decreases by increasing the ratio of S/W to reach its lowest value of  $26.7 \Omega \text{ cm}$  which corresponds to a S/W molar ratio of 24 (WS24 sample). The value of carrier density is low for the WS6 sample, then it was sharply rises to  $7.0 \times 10^{14} \text{ cm}^{-3}$  in the S/W ratio of 12, followed by an increase towards  $6.0 \times 10^{15} \text{ cm}^{-3}$  in the S/W ratio of 24. The substitutional replacement of oxygen by sulfur will generate one extra charge carrier, which will increase the carrier density.

The relative reduction of resistance of the  $WS_2/WO_3$  thin films versus exposure time is shown in Fig. 6. It can be seen that the photoconductivity properties of the films decrease with increasing sulfur concentration. The best photoconductivity properties were obtained for 6 at.% sulfur to tungsten molar ratio.

## 4 Conclusions

$WS_2/WO_3$  binary thin films with different S to W molar ratios ( $[S]/[W] = 6\text{--}24$  at.%) have been prepared by annealing the sprayed layers in sulfur atmosphere. Structural, morphological, optical, electrical and photoconductivity characterizations were performed. It was observed that the physical properties of films were strongly depend on sulfurization and the  $[S]/[W]$  concentration in the spray solution. We found that by changing the  $[S]/[W]$  ratio in the precursor solution and the sulfurization process: (a) according to XRD results, the amorphous nature of as-deposited layers changed to a binary phase crystal correspond to coupled semiconductor  $WS_2/WO_3$ ; (b) differences in surface morphology of the layers as a consequence of increasing the crystal growth rate were observed; (c) transmission of layers where found to decrease after annealing and all the studied samples had high absorption coefficient values higher than  $10^4 \text{ cm}^{-1}$  in the visible region; (d) the direct band gap values related to two transitions of coupled semiconductor decreased from 2.46 to 2.18, and 1.71 to 1.17 eV which correspond to  $WO_3$  and  $WS_2$  phases, respectively; (e) all the studied samples had degenerate  $p$ -type conductivity and the electrical resistivity of the layers decreased from about  $512.5\text{--}26.7 \Omega \text{ cm}$ . The study confirms the presence of two semiconductors with different energy levels for the corresponding conduction and valence bands which probably leads to this enhancement with the displacement of electrons and holes from one semiconductor to another; and (f) the best photoconductive property was obtained for WS6 (S/W = 6 at.%) film.

## References

1. R. Cerc Korosec, P. Bukovec, Acta Chim. Slov. **53**, 136 (2006)
2. C.M. Lampert, Sol. Energy Mater. **11**, 1 (1984)
3. R. Hurditch, Sci. Technol. **3**, 247 (1977)
4. M.G. Hutchins, O. Abu-Alkhair, M.M. El-Nahass, K. Abd El-Hady, Mater. Chem. Phys. **98**, 401 (2006)
5. P. Losier, P.V. Ashrit, J. Mater. Sci. Lett. **22**, 1095 (2003)
6. A.A. Joraid, S.N. Alamri, Phys. B **391**, 199 (2007)
7. M. Regragui, V. Jousseau, M. Addou, A. Outzourhit, J.C. Bernede, B. El Idrissi, Thin Solid Films **397**, 238 (2001)
8. Y. Yamada, K. Tabata, T. Yashima, Sol. Energy Mater. Sol. Cell **91**, 29 (2007)
9. K.D. Lee, Thin Solid Films **302**, 84 (1997)

10. G. Seifert, H. Terrones, M. Terrones, G. Jungnickel, T. Frauenheim, *Phys. Rev. Lett.* **85**, 146 (2000)
11. L. Rapoport, Y. Bilik, Y. Feldman, M. Homyonfer, B.H. Cohen, R. Tenne, *Nature* **387**, 791 (1997)
12. J. Chen, Z.L. Tao, S.L. Li, *Angew. Chem. Int. Ed.* **42**, 2147 (2003)
13. J.W. Chung, Z.R. Dai, F.S. Ohuchi, *J. Cryst. Growth* **186**, 137 (1988)
14. C. Ballif, M. Regula, P.E. Schmid, M. Remskar, R. Sanjines, F. Levy, *Appl. Phys. A* **62**, 543 (1996)
15. A. Klein, S. Tiefenbacher, V. Eyert, C. Pettenkofer, W. Jaegermann, *Phys. Rev. B* **64**, 205416 (2001)
16. J. Li, X.P. Zhao, C.M. Yan, *Mater. Lett.* **60**, 2896 (2006)
17. J.J. Devadasan, C. Sanjeeviraja, M. Jayachandran, *J. Cryst. Growth* **226**, 67 (2001)
18. S.J. Li, J.C. Bernede, J. Pouzet, M. Jamali, *J. Phys. Condens. Matter* **8**, 2291 (1996)
19. S. Jana, P. Bera, B. Chakraborty, B. Chandra Mitra, A. Mondal, *Appl. Surf. Sci.* **317**, 154 (2014)
20. L.J. Van der Pauw, *Philips Res. Rep.* **13**, 1 (1958)
21. J. Tauc, In: J. Tauc (Ed.), *Amorphous and Liquid Semiconductors*, (Plenum, London, 1974)